Journal of Microbiology (2020) Vol. 58, No. 5, pp. 377–386
DOI 10.1007/s12275-020-9365-3
eISSN 1976-3794
pISSN 1225-8873

Full-repertoire comparison of the microscopic objects composing the human gut microbiome with sequenced and cultured communities[§]

Edmond Kuete Yimagou[1], Jean-Pierre Baudoin[1], Rita Abou Abdallah[1], Fabrizio Di Pinto[1], Jacques Yaacoub Bou Khalil[2*], and Didier Raoult[1*]

[1]Aix Marseille Univ., IRD, AP-HM, MEPHI, VITROME, IHU Méditerranée Infection, Marseille, France
[2]Institut Hospitalo-Universitaire Méditerranée-Infection, Marseille, France

(Received Jul 26, 2019 / Revised Feb 11, 2020 / Accepted Feb 11, 2020)

The study of the human gut microbiome is essential in microbiology and infectious diseases as specific alterations in the gut microbiome might be associated with various pathologies, such as chronic inflammatory disease, intestinal infection and colorectal cancer. To identify such dysregulations, several strategies are being used to create a repertoire of the microorganisms composing the human gut microbiome. In this study, we used the "microscomics" approach, which consists of creating an ultrastructural repertoire of all the cell-like objects composing stool samples from healthy donors using transmission electron microscopy (TEM). We used TEM to screen ultrathin sections of 8 resin-embedded stool samples. After exploring hundreds of micrographs, we managed to elaborate ultrastructural categories based on morphological criteria or features. This approach explained many inconsistencies observed with other techniques, such as metagenomics and culturomics. We highlighted the value of our culture-independent approach by comparing our microscopic images to those of cultured bacteria and those reported in the literature. This study helped to detect "minimicrobes" Candidate Phyla Radiation (CPR) for the first time in human stool samples. This "microscomics" approach is non-exhaustive but complements already existing approaches and adds important data to the puzzle of the microbiota.

Keywords: microscomics, culturomics, metagenomics, gut microbiome, minimicrobes, repertoire

Introduction

Creating an exhaustive repertoire of the human microbiome components remains a challenging objective (Lagier *et al.*, 2012; Hugon *et al.*, 2013, 2017). The human microbiome consists of the microorganisms living in or on the human body (Whitman *et al.*, 1998; Lloyd-Price *et al.*, 2016). Microorganisms are especially abundant in the human gut, and the composition of the gut microbiome varies with physiological conditions, such as age, geographical origin, and external factors, such as dietary habits (Holdeman *et al.*, 1976) and the use of antibiotics or probiotics (Hugon *et al.*, 2017). In the past few years, specific alterations in the gut microbiome were found to be associated with various pathologies, such as obesity, inflammatory disease, intestinal infection and colorectal cancer (Clemente *et al.*, 2012; Weir *et al.*, 2013).

Accessing the human gut microbiome remains a particular issue. Although stools can be considered waste material, they represent an indirect way to obtain easy access to gut microbiome components and are appropriate for the search for pathological dysregulations (Lagier *et al.*, 2017). Several approaches have been developed to characterize the indigenous gut microbiota: culture-based, later renamed culturomics (Lagier *et al.*, 2012), as well as high-throughput deep-sequencing methodologies (Lagier *et al.*, 2016; Nibali and Henderson, 2016; Hugon *et al.*, 2017). Although 16S RNA sequencing has given us new insight into the microbiota, these different approaches have yielded contradictory results, highlighting the absence of a satisfying global approach capable of listing all the components of the gut microbiota. A list of the gut microbiota components can be provided by microscopy, which is a complementary method that provides images of all the biological objects contained in stool samples. For centuries, microscopy has played an important role in human gut exploration, providing a catalog of the gut microbiota. (Allen *et al.*, 2011), or *in situ* in healthy or infected animals (O'Toole *et al.*, 2004; Earle *et al.*, 2015; Geva-Zatorsky *et al.*, 2015; Propheter and Hooper, 2015). However, the resolution limit of light microscopy prevents us from obtaining ultrastructural details of the fine subcellular components of the microbiome. Transmission electron microscopy (TEM) is the only tool that can provide access to the ultrastructure of micrometer-sized cells (Costerton, 1979). In humans, TEM has been used since the 1960s to investigate human epidermal samples, tooth surfaces, and oral and vaginal mucosa (Scott *et al.*, 1989; Paul *et al.*, 1993; Villegas *et al.*, 1997; Arora and Chapman, 2000; Nibali and Henderson, 2016). Regarding the gut microbiota *per se*, TEM has been especially used *in situ* directly on dissected gut tissue in insects (Breznak and Pankratz, 1977), fish (Ringø *et al.*, 2001, 2003, 2007) and mammals (Mantani *et al.*, 2015) and in humans on gut biopsies of patients with AIDS (Hovind- Hougen *et al.*, 1982; Connolly *et al.*, 1991; Leite *et al.*, 2013), and three studies used TEM to

*For correspondence. (D. Raoult) E-mail: didier.raoult@gmail.com; Tel.: +33-4-13-73-24-01 / (J.Y. Bou Khalil) E-mail: boukhaliljacques@gmail.com
[§]Supplemental material for this article may be found at http://www.springerlink.com/content/120956.

image or explore the microbiome of human stool samples (Browne *et al.*, 2016; Hugon *et al.*, 2017).

In the present study, we used a culture-independent approach and took advantage of the strengths of TEM imaging to elucidate ultrastructural features of all biological objects present in ultrathin sections of resin-embedded stool samples, thus creating a unique repertoire of the gut microbes present in stool samples. The terminology "microscomics" is reported for the first time herein as a new approach that will be complementary to the previous "omics" such as "culturomics", "proteomics", and "metagenomics". This assay is a microscopic approach processed at a large scale for the study of the microbiome. We were particularly interested in investigating CPR, a new domain of life that represents 15% of the domain Bacteria in the oral cavity and has not yet been described in the stool. After acquiring hundreds of micrographs, we sorted all cell-like objects present in the ultrathin sections based on morphological criteria only, such as cell body diameter, cell body density, internal elements, the peripheral membrane or peripheral cell wall structure, and peripheral elements. We sorted objects into 32 distinct morphological categories or morphotypes (Arora and Chapman, 2000), some of which may have contained previously undescribed microorganisms. We also performed a comparison based on the Gram staining of the objects between our TEM data in our "microscomics" approach and the data obtained from light microscopy and metagenomics approaches. We finally compared our "microscomics" catalogue to the ultrastructural features of the most abundant bacteria found by metagenomics, culturomics or both approaches to establish a correlation between these techniques and to emphasize the advantages of the new "microscomics" approach.

Materials and Methods

Stool sample collection

Fresh stool samples were collected from 8 volunteer donors in our laboratory. We labeled these samples *Megagut* 1 to 8, where Megagut stands for the whole microbiome representing the microbial community present in the stool. Donors signed written consent, and the project received ethics committee approval under the number IHU-2016-011. No clinical manifestations of diarrhea were observed in any subject. Volunteers had no antibiotics or any other treatment 6 months prior to sampling. Fecal samples were distributed into 1-gram aliquots at the time of collection and were either frozen at -80°C upon receipt or used as fresh samples. Aliquots of unfrozen stool samples were used for electron microscopy.

Electron Microscopy: Resin embedding, Ultramicrotomy, and Transmission Electron Microscopy (TEM)

Stool samples were fixed in 2.5% glutaraldehyde in 0.1 M cacodylate buffer overnight at 4°C. Samples were washed three times for 10 min with 0.2 M saccharose in 0.1 M cacodylate buffer. Samples were postfixed for 1 h at room temperature with 1% osmium tetroxide in 1.25% potassium ferrocyanate/0.1 M cacodylate solution. Samples were washed three times for 10 min with distilled water and gradually dehydrated with increasing concentrations of ethanol in water: 25, 50, 75, 90, 99, and 100% ethanol for 10 min, 3 min, 3 min, 10 min, 10 min, and 30 min, respectively. Resin substitution was achieved by incubating the samples in successive 15-min intervals in mixtures of Epon812 resin and 100% ethanol solution, with the respective proportions of 25%/75%, 50%/50%, 75%/25%, and overnight in 100% Epon812 resin. Finally, samples were placed in 100% fresh Epon812 resin, and polymerization was achieved at 60°C for 3 days. Between all these steps, the samples were ultracentrifuged at 5,000 × *g*, and the supernatant was discarded. Ultrathin sections (70 nm) were cut on a UC7 (Leica) ultramicrotome and deposited on 300 mesh copper/rhodium grids (Maxtaform HR25, TAAB). For each sample, three sections were collected each time at 10 µm apart in the depth of the resin inclusion blocks to cover a large and diverse area of the sample. Sections were poststained with 5% uranyl acetate and lead citrate according to the Reynolds method (Reynolds, 1963). Electron micrographs were obtained on a Tecnai G^2 transmission electron microscope (FEI) operated at 200 keV equipped with a 4,096 × 4,096 pixel resolution Eagle camera (FEI). Magnification ranged between X 14,000 and X 25,000.

Metagenomic sequencing

Samples were extracted in two kinds of lysis protocols: one with protease and the other including deglycosylation steps, both detailed in the work of Angelakis *et al.* (2016). Afterwards, pooling, barcoding, and 16S rRNA sequencing were performed as follows. Briefly, for each protocol, metagenomic DNA was amplified for the 16S "V3-V4" regions by PCR for 40 cycles using Kapa HiFi Hotstart ReadyMix 2x (Kapa Biosystems Inc.), and the surrounding conserved region V3_V4 was amplified with primers with overhang adapters, RevOvAd_785R GTCTCGTGGGCTCGGAGATGTGTAT AAGAGACAGGACTACHVGGGTATCTAATC. After purification on AMPure beads (Beckman Coulter Inc.), the concentration was measured using high sensitivity Qubit technology (Beckman Coulter Inc.), and the DNA was diluted to 1 ng/µl. At this step, the library of protocol 1 was pooled volume to volume to the library of protocol 5 so that the subsequent limited cycle PCR was performed with 15 ng DNA, and Illumina sequencing adapters and dual-index barcodes were added to the amplicon. After purification on AMPure beads (Beckman Coulter Inc.), this library was pooled with 95 other multiplexed samples. The global concentration was quantified by a Qubit assay with a high sensitivity kit (Life Technologies). Before loading for sequencing on MiSeq (Illumina Inc.), the pool was diluted to 7 pM. Automated cluster generation and paired-end sequencing with dual index reads were performed in a single 39-h run in a 2 × 250 bp.

Bacterial species used as morphological references for method validation

We used the nine most abundant bacterial species found in common in both metagenomic and culturomic approaches (Lagier *et al.*, 2015) on the eight Megagut stool samples to correlate these bacterial morphological structures to our 32 categories. These nine bacteria were pure and underwent the same experimental procedures regarding embedding, sec-

tioning and TEM screening and observations, as described previously. We compared each pure bacterial morphotype to our 32 categories. We looked for a relationship/link between microscomic categories and the top pure bacterial morphology or structures. We also used images of species described in the literature.

Gram staining and light microscopy

One gram of unfrozen stool sample was diluted in 200 µl of PBS, spread on a glass slide with an inoculation loop and dried over a gentle flame. We then carried out heat-fixed preparations with the Gram staining technique, which is routinely used in our laboratory and many other microbiology labs. The slides were observed at 100X (oil immersion) magnification (HCX, PL, and PH 3CS) with a numerical aperture of 1.4 using a DMI 6000 (Leica) inverted microscope in bright-field mode. A minimum of 500 cells per slide were counted for positive or negative Gram stain results. The Cell Counter plugin in ImageJ (NIH) was used for cell counting.

PCR targeting Candidate Phyla Radiation (CPR)

DNA extraction was performed using the EZ1® DNA Tissue Kit as recommended by the provider (Qiagen), and PCR was performed with 25 µl of Taq (Ampli Taq Gold), 18 µl of water, 1 µl of each primer M-7580F; TM7-1177R (Takenaka *et al.*, 2018) with a concentration of 0.60 µM and 5 µl of DNA. The following program was used for amplification by DNA Taq polymerase: initial denaturation at 95°C for 15 min, denaturation at 95°C for 5 min, annealing at 63°C for 1 min, extension at 72°C for 5 min, and final extension at 15°C for 10 sec. Electrophoresis was performed in a 1.5% agarose gel, and the gel was examined under a UV lamp (E-gel imager, Life Technologies). PCR products were purified with a NucleoFast plate (Macherey-Nagel) followed by the sequencing process. Sequences were further analyzed by Chromas Pro software.

Statistical analysis

Statistical analyses were performed using SPSS software version 22. Means and standard deviations are shown for quantitative variables. Two-sided statistical tests were used for comparisons between groups. Since we had more than two groups and the variations were nonhomogeneous, the Kruskal Wallis test was used, which is the nonparametric equivalent of the one-way ANOVA test. Student's t-test was used to compare two means, and a p-value less than 0.05 was considered significant. The Spearman correlation coefficient was used to correlate quantitative variables.

Results

Ultrastructure repertoire and defined categories of Megagut stool sample components by the microscomic approach

After embedding Megagut stool samples in Epoxy resin following standard protocols, we made ultrathin sections by collecting sections 10 µm apart at the depth of the inclusion block to avoid repetitive observations of the same object. For each of the 8 samples, we observed 3 ultrathin sections, capturing each of the objects of interest. An object was considered of interest, further considered as a cell and analyzed in detail if it enclosed material surrounded by a single or several wall(s) or closed peripheral membrane(s). Classification of the objects/cells was based on 1) the diameter of the cell body, 2) the density of the cell body, 3) the internal elements, 4) the structure of the peripheral membrane or peripheral wall, and 5) the peripheral elements. The shape of objects was not considered an important criterion. Indeed, a bacillus or a coccus section located in some areas could look similarly round-shaped even if the gross morphology of the whole cells differed. When we looked at the ultrathin sections, objects appeared more or less clustered among regions. Some tissue fractions, such as micrometer-sized debris or larger (more than 10 microns), were also found in sections. We acquired a mean number of 505 ± 143 (n = 8) objects per stool sample (Supplementary data Table S1), representing a total number of 4,038 objects.

Based on morphological criteria, we sorted objects into 32 ultrastructural categories (Fig. 1). These categories included the single or several morphological criteria explained below. We used the term 'morphotype' to name these categories (Arora and Chapman, 2000).

Two specific categories were made regarding cell diameter: 1) cells with a maximum diameter below 300 nm (category 32, Figs. 1 and 2) cells with a maximum diameter above 3 µm (category 22, Fig. 1). Cells with a maximum diameter between 300 nm and 3 µm were not sorted into a specific diameter category. The shapes of objects from category 32 with a diameter less than 300 nm (Fig. 1) did not correspond to the typical symmetrical morphology of viruses but rather bacterial morphologies, with typical surrounding membranes.

The cell body was classified as hyper or hypodense. Hyperdense objects showed an electron-dense cell body, in general, completely filled with material. In comparison, hypodense cells had a lesser electron-dense cell body, generally containing electron-lucent regions lacking material. The internal cytoplasm was classified as smooth or granular. In smooth cytoplasm cells, the electron density was homogeneous, whereas in granular cells, darker thick electron-dense spherical spots were present in some areas of the cytoplasm or in the whole cytoplasm (category 13, Fig. 1). These thick granules were different from the thinner dispersed grains found in the category 'disc with grains' (category 5, Fig. 1). The internal elements, when present, were classified as intracytoplasmic compartments, internal membranes, mesosomes, detached membranes, inclusions, vacuoles, or dense bodies. Intracytoplasmic compartments (category 2, Fig. 1) corresponded to double membranes enclosing an internal compartment. Internal membranes differed from internal compartments, as they did not clearly enclose a region inside the cell bodies. Mesosomes corresponded to peripheral membranes reaching the central parts of the cell inside the cytoplasm (category 16, Fig. 1). Detached membranes corresponded to distinct membranes below the cell wall, superposed to the inner membrane of the cell wall and further detached from it (category 29, Fig. 1). Inclusions corresponded to spherical compartments differing from the vacuoles by their electron-dense characteristics (category 9, Fig. 1). Vacuoles corresponded to round electron-

lucent structures (category 19 and 23, Fig. 1). Condensed cells possessed diffuse central electron-dense regions with a cytoplasm not enclosed by a membrane (category 8, Fig. 1), and dense bodies referred to the same type of material, except that the electron-dense material was smaller and more concentrated inside the cell (category 11, Fig. 1).

The double membrane at the periphery of the objects was classified as thin or thick, ranging from a few nanometers (category 25, Fig. 1) to 50 nm (category 24, Fig. 1) between the two membranes, respectively. When we observed more than one double membrane, the so-called peripheral wall was classified according to the Gram definition, when possible. Gram-positive cells (Gram+) possessed a single peripheral double membrane below an outer thick electron-dense layer (category 15 and 28, Fig. 1). Gram-negative cells (Gram-) possessed an inner double membrane, an outer double membrane and a thin electron-dense layer in-between (category 6 and 27, Fig. 1). Cells with a cell wall not recognizable as Gram-positive or Gram-negative were sorted into the 'undefined' category. The aspect of the peripheral wall was also sorted into specific categories if its shape was not straight and regular, such as serrated (category 3, Fig. 1), zipper-like (category 21, Fig. 1), or wavy (category 30, Fig. 1). A category was made for objects with no distinguishable peripheral wall or peripheral single membrane and was referred to as the discoid category (category 4, Fig. 1). In this category, the objects were round and filled with homogeneous densities of cytoplasmic-like material.

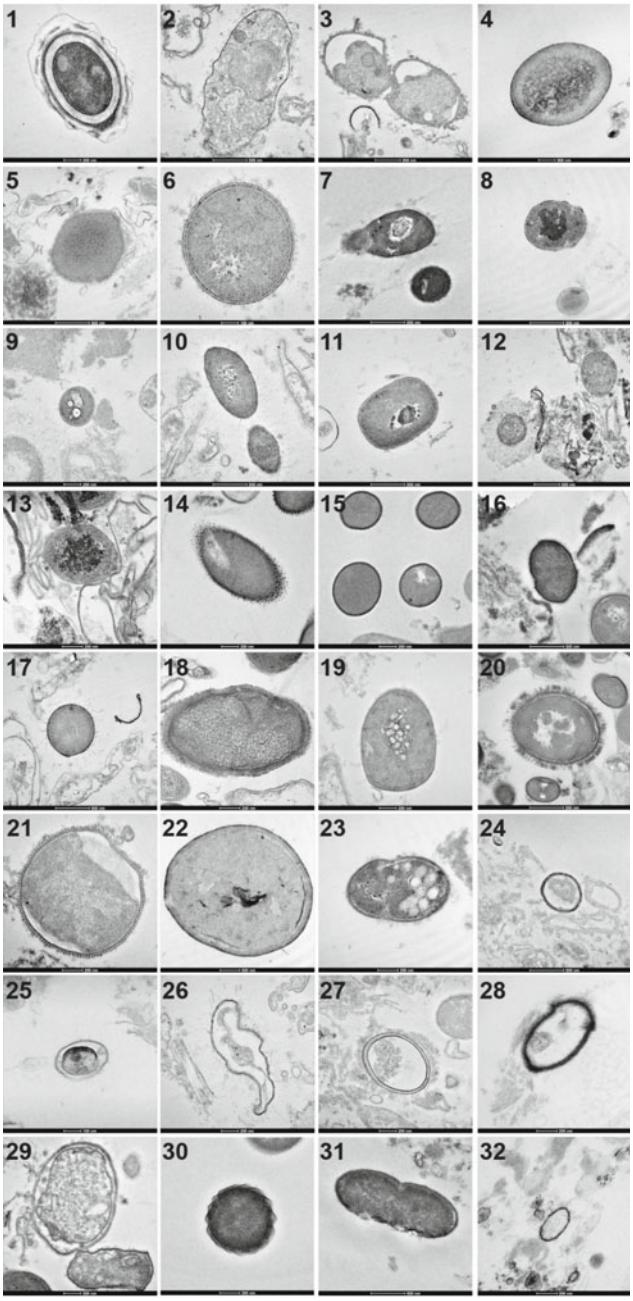

Fig. 1. TEM reference images of the 32 ultrastructural categories (morphotypes) found in the stool samples.
1. Hyperdense sporulated
2. Hyperdense internal compartment
3. Hyperdense serrated
4. Hyperdense discoïd
5. Hyperdense disc with grains
6. Hyperdense Gram-
7. Hyperdense Gram- hairy
8. Hyperdense Gram+ condensed
9. Hyperdense Gram+ with dense bodies and inclusions
10. Hyperdense Gram+ with dense bodies and spicules
11. Hyperdense Gram+ with dense bodies
12. Hyperdense Gram+ with envelope
13. Hyperdense Gram+ granulated
14. Hyperdense Gram+ spiky
15. Hyperdense Gram+
16. Hyperdense Gram+ with spicules and mesosomes
17. Hyperdense Gram+ with spicules without mesosomes
18. Hyperdense Gram+ hairy
19. Hyperdense Gram- with vacuoles
20. Hyperdense with brushy hair
21. Hyperdense with zipper membranes
22. Hyperdense with diameters greater than 3 µm, thick wall
23. Hyperdense Gram+ with vacuoles
24. Hypodense double thick membrane
25. Hypodense double thin membrane
26. Hypodense double membrane with spicules
27. Hypodense Gram-
28. Hypodense Gram+
29. Detached membranes
30. Wavy membrane
31. Dividing
32. Diameters less than 300 nm

Pictures: 6, 25. Scale bars = 100 nm
Pictures: 1,9, 13, 14, 15, 18, 19, 21, 23, 26, 27, 28, 29, 30, 32. Scale bars = 200 nm
Pictures: 2, 3, 4, 5, 7, 8, 10, 11, 12, 16, 17, 20, 22, 24, 31. Scale bars = 500 nm

Peripheral elements, when present, were classified as thin spicules (categories 16, 17, and 26, Fig. 1), thick spikes (hedgehog-like; category 14, Fig. 1), hairy envelopes (categories 7 and 18, Fig. 1), brushy hair envelopes (category 20, Fig. 1) or homogeneous envelopes (category 12, Fig. 1). Dividing cells were grouped into a category (category 31, Fig. 1), corresponding to cells with a cell body possessing a central constricted region. 'Sporulating' cells were also grouped together (category 1, Fig. 1), corresponding to cells with peripheral membrane stacks surrounding a central electron-dense region.

Following this classification, we used our qualitative catalog of the morphotypes present in the Megagut samples to quantify the number of objects present in each sample. The results of the morphotype distribution for each of the 8 Megagut samples are listed in Supplementary data Table S1. A graphical representation of one Megagut sample (Megagut4) is shown in Fig. 2. Morphotypes are listed in Figs. 1 and 2 according to the density of the cell body: hyperdense objects first (categories 1-23, Fig. 1; dark-gray panel in Fig. 2), then hypodense objects (categories 24-28 Fig. 1; light gray panel in Fig. 2) and finally 'other' morphotypes (categories 29-32 Fig. 1; white panel in Fig. 2). The respective abundance of each cell body density class for the 8 Megagut stool samples is illustrated in Supplementary data Fig. S1. On average, we found 71 ± 11% hyperdense cells, 15 ± 10% hypodense cells, and 14 ± 4% 'other' cells among the 8 samples.

Our quantification of the ultrastructural categories showed that each morphotype was found in at least two Megagut samples (Supplementary data Table S1). Out of the 32 morphotypes, 11 morphotypes were found in common in all 8 Megagut samples: morphotypes 1, 4, 5, 12, 15, 18, 27, 29, 30, 31, and 32. The abundance between each morphotype among the 8 Megagut samples was compared, which showed a p-value less than 0.001. The main difference resided in morphotypes 1, 12, and 17, which corresponded to hyperdense sporulated cells, hyperdense Gram+ cells with a peripheral envelope and hyperdense Gram+ cells with spicules, respectively (Supplementary data Fig. S2).

Gram analysis of the Megagut stool samples by "microscomics" and its comparison to light microscopy and metagenomic approaches

Since Gram staining may sometimes lead to bacterial misidentification due to the staining variability of some bacteria (Hugon *et al.*, 2013), we decided to resolve the Gram nature of the microbes present in the Megagut stool samples. For this, we compared our microscomic TEM data to data from classical Gram staining and from metagenomics.

Gram nature and microscomic analysis : We analyzed the distribution of the morphotype categories based on three large groups composed of either Gram-positive objects, Gram-negative objects or objects with unclear Gram characterization ('other' category). The results are shown in Supplementary data Fig. S3. Overall, the distribution of the Gram-positive, Gram-negative and 'other' categories was homogeneous among the 8 Megagut stool samples: the mean abundance of Gram+, Gram- and 'other' objects was 57 ± 5%, 19 ± 4% and 24 ± 5%, respectively. Abundances between Gram+ and Gram- and between Gram+, Gram-, and the 'other' objects were significantly different ($p < 0.005$). The ratio (%Gram+/%Gram-) was equal to 3.0.

Gram staining and light microscopy analysis : We performed Gram staining on all eight samples followed by light microscopy, and we counted a total of 5,469 cells for the 8 Megagut samples on 3 images for each sample on average. A representative image of the stained Megagut 4 sample is shown in Supplementary data Fig. S4. The mean number of Gram+ cells was 420 ± 63, and the mean number of Gram- cells was 307 ± 36 cells, on average, corresponding to mean abundances of 62 ± 5% and 38 ± 5%, for Gram+ and Gram-, respectively. Mean abundances between Gram+ and Gram- cells were significantly different ($p < 0.01$). The ratio (%Gram+/%Gram-) was equal to 1.6.

Gram and metagenomic analysis : By metagenomics, we found a mean number of 135 ± 18 known bacterial species and a mean number of 1,674 ± 905 unknown bacteria at the species level per sample (Supplementary data Table S2). The known bacterial species thus represented only a very small

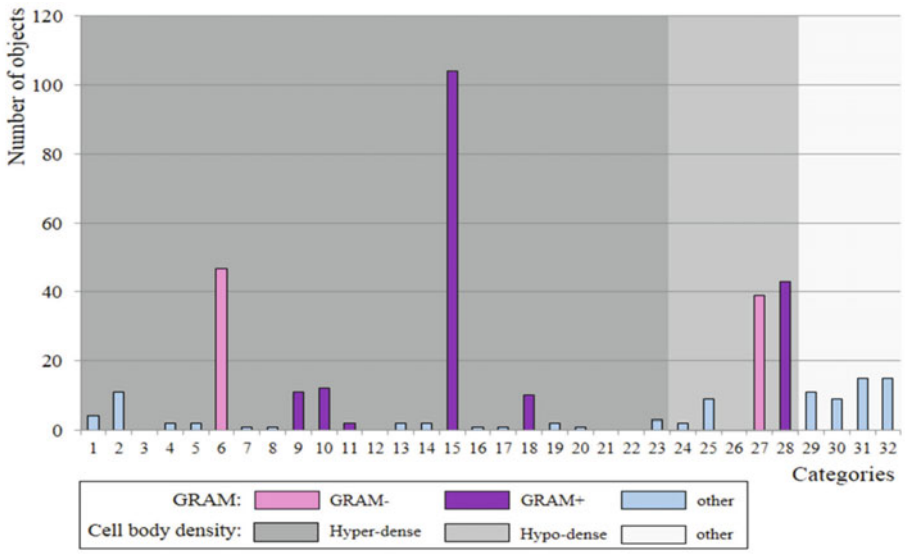

Fig. 2. Distribution of the objects found in stool sample 4 among the morphotype categories.

fraction of the total bacterial species present in the samples (8% versus 92%, on average; Supplementary data Table S2). Among the bacteria known at the species level in each of the 8 stool samples, given the respective metagenomic abundance of each species, we calculated the percentage of the top 10 most abundant species for the 8 samples. Among the 8 samples, the top 10 species represented on average 73.9 ± 5.8%. These top 10 known bacterial species of each sample could be found in only one sample but also in several samples: after merging all these species, we obtained a total of 35 core microbiome species (Supplementary data Table S3). These 35 core-microbiome species represented among the 8 samples a mean abundance of 86 ± 2% of the total bacteria species. Statistically, the abundances of these 35 core bacterial species in all 8 samples were different (P-value < 0.001). The main difference resided in the top species, *Bifidobacterium faecale*. Principal component analysis (PCA) of the 35 top bacterial species from the 8 studied stool samples showed that *Bifidobacterium faecale*, *Romboutsia timonensis*, and *Akkermansia muciniphila* are a group separated from the rest of the other bacterial species (Supplementary data Fig. S5). There was no significant difference between the top 1 *Bifidobacterium faecale*, top 2 *Romboutsia timonensis*, and top 3 *Akkermansia muciniphila* bacteria species (Supplementary data Table S3). These results were in concordance with the statistical analysis shown in Supplementary data Table S3. For each stool sample, we calculated the abundance of each Gram category regarding the number of species it contained versus the total number of known species. (Fig. 3 and Supplementary data Table S4) and found the following values: 62 ± 7.5% Gram+ species, 36.9 ± 6.8% Gram- species and 1.1 ± 1.1% of other species (Gram variable or archeobacteria). The comparison of the number of bacterial species among the Gram categories showed a significant difference (p-value inferior to 0.001), where Gram+ species were more represented than Gram- species (Supplementary data Table S4).

We also calculated the cumulated number of reads/hits of known bacterial species of each Gram category for each stool sample, i.e., the actual number of known bacteria, corresponding either to the Gram+, Gram- or 'other' group (Supplementary data Table S5). We found that the average abundances of each class of Gram regarding the number of bacteria were 68.8 ± 24.6% for Gram+, 30.3 ± 24.3% for Gram- and 0.9 ± 1.6% for bacteria of unknown Gram characterization or archeobacteria. The ratio (%Gram+ bacteria/%Gram- bacteria) was equal to 2.3 (Fig. 3 and Supplementary data Table S5).

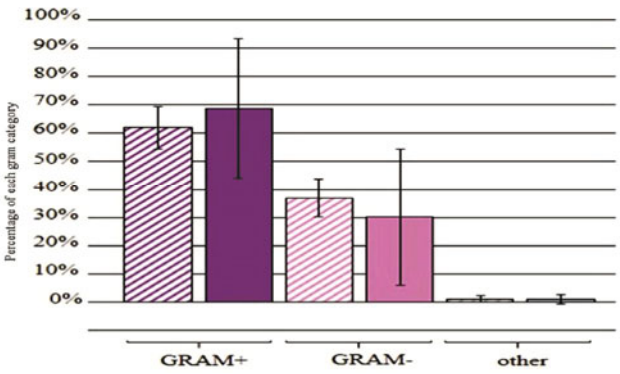

Fig. 3. Mean Gram distribution among the 8 stool samples by metagenomics. Mean abundance of the bacterial species regarding their Gram category (dashed bars), regardless of the number of bacteria, and the mean abundance of bacteria of each Gram category, regardless of their species (full bars).

Correlation between microscomic categories/morphotypes and known microbial ultrastructures

To compare our microscomic repertoire to the ultrastructural features of frequent bacteria found in the Megagut samples by metagenomics and/or culturomics, we chose 9 specific bacterial species (Supplementary data Table S6 and Fig. 1). First, we chose bacterial species found among the 35 core metagenomic species (Supplementary data Table S3), which were also found by the culturomic approach (Lagier *et al.*, 2015). We chose *Escherichia coli*, *Bacteroides vulgatus*, *Bifidobacterium longum*, *Holdemanella biformis*, *Lactobacillus ruminis*, *Methanobrevibacter smithii*, and *Streptococcus salivarius*. Then, to study the bacillus and clostridium genera present in the 35 core metagenomic bacteria (*Bacillus tequilensis* and *Clostridium saudii*), we also studied *Bacillus massiliensis* and *Clostridium amazonitimonensis*. For the remaining bacteria, we looked for their micrographs in the literature and tried to link their morphology to our classified categories.

We performed TEM analysis of the 9 selected pure bacterial species, and we found between one and three microscomic morphotypes for each species. The results of this analysis are listed in Supplementary data Table S6 and representative images are shown in Fig. 4. Out of the 32 microscomic categories, 14 morphotypes were found in the micrographs of the 9 selected bacteria. Among these 14 morphotypes, each morphotype was found in one to four bacterial species. The most represented morphotypes were numbers 15 and 28, hyperdense Gram+ and hypodense Gram+ cells.

Molecular biology targeting CPR

Among the 8 stools tested, stool sample 1, which showed a

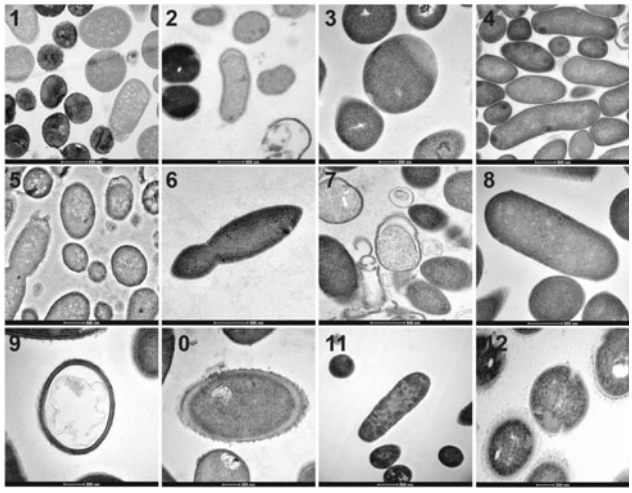

Fig. 4. Morphotypes of cultured bacterial strains.

percentage of 2.5% of objects corresponding to category or morphotype 32, was PCR positive with a 600 base pair band. After sequencing, the PCR material of stool sample 1 revealed the phylum TM7 Saccharibacteria.

Discussion

Our unique TEM image repertoire initiated both qualitative and quantitative analysis of the objects present in stool sections. We established a repertoire of diverse objects based on morphological features. We showed a clear difference in the level of distribution and diversity among the tested healthy individuals. The microscomic approach suggests that the Gram+ population is more abundant than what was shown by conventional Gram staining or metagenomic profiling (Fig. 5): the ratio between the mean abundances of Gram+ and Gram- bacteria among the 8 stool samples for Gram staining, metagenomics and "microscomics" was 1.6, 2.3, and 3.0 respectively (Fig. 5). If Gram+ bacteria from old cultures appeared or stained as Gram-negative (Taras *et al.*, 2002), we avoided such Gram staining artifacts linked to the age of culture as we stained uncultured stool samples. The discordance between metagenomics and "microscomics" can be explained herein as follows. First, the anomaly detected by Hugon *et al.* (2013) between the number of Gram- and Gram+ phyla was recently explained by the fact that a significant number of Firmicutes, which are supposed to be Gram+, are Gram-. Thirty-two orders and four families in the negativicutes (such as Veillonellales, *Acidaminococcales*, and *Selenomonadales*) represent a large part of the gut microbiota, which can explain why the microscomic approach found a higher proportion in Gram classification than the one found by metagenomics. Another discrepancy can also be due to the DNA extraction process, especially for bacteria with a thick cell wall, which are less represented. Other bacteria are also less represented by metagenomics, where some inhibitors, such as sugar and biofilms, inhibit proteolysis and thus DNA extraction (Angelakis *et al.*, 2016).

This approach allowed many discoveries, mainly that of morphotype 32, characterized by objects with a diameter below 300 nm (Morphotype 32; Fig. 1), that are highly correlated or matched with the Candidate Phyla Radiation (CPR), a recently described expansion of the tree of life that represents more than 15% of all bacterial diversity with an ultrasmall cell size (200–300 nm) (Danczak *et al.*, 2017; McLean *et al.*, 2018). This makes our study the first to illustrate the presence of CPR in stools since all previous studies detected these microorganisms only in the oral cavity and in the environment. Regarding these results and images, we used molecular biology to target CPR and confirmed our findings by specific and positive PCR results (Fig. 6). In addition, correlative microscopy using targeted probes is an ongoing method to validate and quantify CPR in stools. This study showed the importance of this approach to detect bacteria previously undetected by culture or Gram staining.

We did not observe any structure resembling a flagellum of bacteria in the *Lactobacillus* or *Clostridium* genera (categories 1,4,8,9,10, Fig. 4), although some species from the metagenomic top core microbiome (Supplementary data Table S3) represented bacteria with a flagellum: *Lactobacillus ruminis* and *Clostridium saudii* (Southern, 1975; Gatson *et al.*, 2006; Forde *et al.*, 2011; Angelakis *et al.*, 2014). Thus, when cut into ultrathin sections, flagella might not be clearly recognizable, at least with our method. "Microscomics" suggests that there might be differences between stool gut-derived cells and cells in culture regarding their morphology and their environment, where most bacterial ultrastructures mentioned in the literature are obtained from cultures and not directly derived from samples. We did not find the corresponding morphotype (12) for *Bacteroides vulgatus* and *Methanobrevibacter smithii* (categories 2 and 11, Fig. 4). Capsules were only found for *Streptococcus salivarius* (categories 11, Fig. 4). This was the same result for spore-forming bacteria that are most likely represented by category 1 (hyperdense sporulating; Fig. 1), with a mean abundance of 9.1%. The cumulative abundance based on metagenomics of spore-forming bacteria (*Clostridium saudii* and *Bacillus tequilensis)* represents 4.5%. No spores were detected in cultured *Bacillus massiliensis* or *Clostridium amazonitimonensis*, although they are sporulating species. Culture conditions such as nutrient availability may influence spore formation, as may the gut microbiota (Serra *et al.*, 2014; Meeske *et al.*, 2016). In our TEM images of cultured *Bacillus massiliensis* (categories 1, Fig. 4),

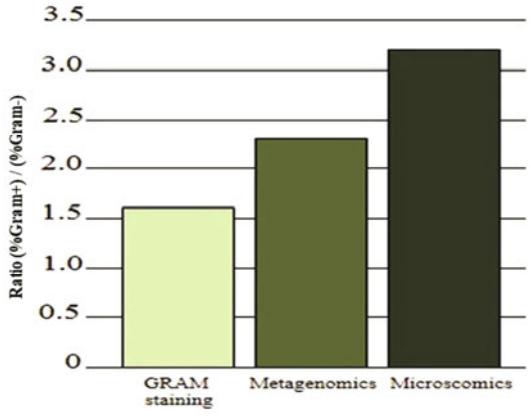

Fig. 5. **Ratio (%Gram+)/(%Gram-) of the classical Gram staining technique and of metagenomics and "microscomics" approaches.**

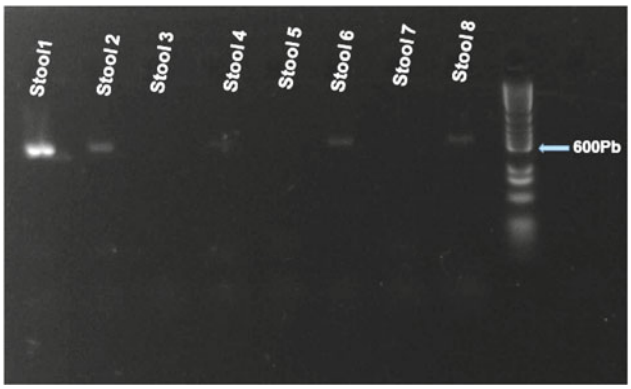

Fig. 6. **Amplification of stool sample PCR products.**

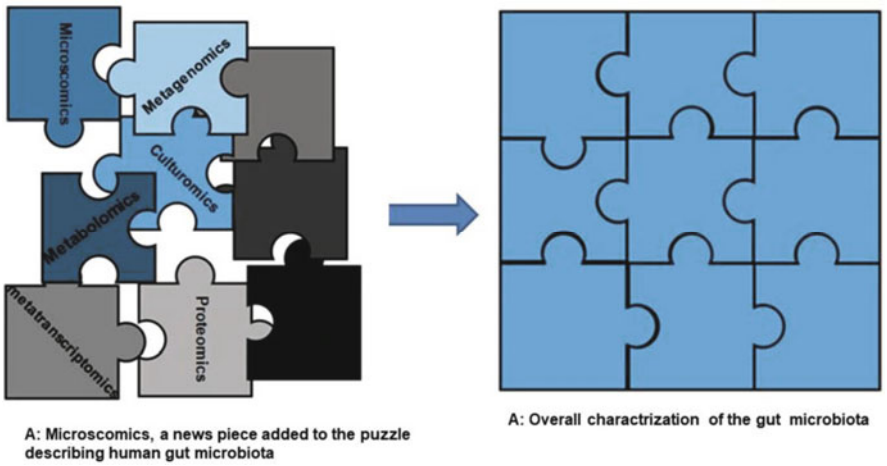

Fig. 7. "Microscomics", a new approach to study the human gut microbiota

these morphotypes were nevertheless not found. Regarding 'dividing' cells, the mean abundance of morphotype 31 in "microscomics" was low (2.1 ± 2.2%; Fig. 1) compared to its abundance in cultured cells (up to 30%; Supplementary data Table S6). The extent to which morphologically dividing cells in stools represent the actual proliferation rate of the microbiome *in situ* remains to be explored. Comparing the images to known cell types is useful considering that many external factors (such as cell cycle and metabolic state) other than taxonomy also affect cell morphology. Regarding ultrastructural similarities, we found hypodense cells that likely correspond to dead cells prior to chemical fixation, except for morphotype 25, which may include mycoplasma cells that can present a thin single double-membrane and a hypodense internal compartment (Sato *et al.*, 2012). Hypo-dense cells were also present in the TEM images of cultured bacteria (categories 1, 4, 7, and 9, Fig. 4). *Akkermansia muciniphila* and *Faecalibacterium prausnitzii*, the top 3 and top 6 bacterial species of the core microbiome (Supplementary data Table S3), were reported to be key markers of a healthy gut (Dao *et al.*, 2016; Ferreira-Halder *et al.*, 2017). The abundance of morphotypes that are likely to correspond to these bacteria (morphotypes 27 and 18, Fig. 1) corroborates the healthy status of our individuals.

The wavy-membrane objects in microscomics (category 30, Fig. 1) were found for cultured *Escherichia coli* and *Lactobacillus ruminis* [Fig. 4(5); Fig. 4(8–10)]. Morphotype 30 also resembles the morphology of *Ruminococcus obeum* (see Fig. 4 in [Browne *et al.*, 2016]). This morphotype may group non-sporulating bacteria of several species. Morphotype 16 (Fig. 1) was closely linked to the *Bifidobacter* family, with *Bifidobacterium faecale* (top 1) and *Bifidobacterium longum* subsp. *longum* (top 13) from metagenomic studies (Supplementary data Table S3). Indeed, mesosomes are morphological features often observed in *Bifidobacter* strains (Bauer *et al.*, 1975), and TEM images of cultured *Bifidobacterium longum* showed these mesosomes [Fig. 4(3)].

Hyperdense objects with a diameter beneath 3 μm and a thick wall (morphotype 22, Fig. 1) may include radio-resistant bacteria such as *Geodermatophilus* (Ivanova *et al.*, 2010) or larger eukaryotes such as yeasts (Walker *et al.*, 2010). It has been shown that yeasts represent 0,001 to 0.01% of the human mycobiome (Nash *et al.*, 2017; Auchtung *et al.*, 2018). The internal compartment of the objects from morphotype 2 (hyperdense internal compartment; Fig. 1) is likely indicative of cells with a nucleus and thus may include eukaryotic cells as well as planctomycetes eubacteria cells (Santarella-Mellwig *et al.*, 2010; Fuerst and Sagulenko, 2011; Pinos *et al.*, 2016).

Finally, to our knowledge, the nature of the objects found for morphotypes 3 (hyperdense serrated), 14 (hyperdense Gram+ spiky), 20 (hyperdense with brushy hair), and 21 (hyperdense with zipper membranes) (Fig. 1) is still unknown.

Our "microscomics" approach is unique, as it provides a whole repertoire of gut-derived microbiome components, with no dependence on cell culture or staining interpretation. Our "microscomics" approach showed that the abundance of Gram+ cells in the analyzed stool samples was probably underestimated after classical Gram staining and metagenomics approaches. It showed cellular ultrastructures typical of known bacterial species but also previously undescribed morphologies, which may belong to unknown microorganisms. This approach is complementary to other "omics" disciplines used in microbiota studies, mainly culturomics and metagenomics. It will bring new insight and clear many unresolved problems that culturomics and metagenomics have raised. This representative and non-exhaustive method is complementary and supplements the understanding of the gut microbiota (Fig. 7). Future progress in correlating transmission and/or scanning electron microscopy data to precisely identify the objects present in ultrathin sections of stool samples will help utilize our approach to obtain a full repertoire of the cells present in the gut microbiome. Fluorescence in situ hybridization-FACS (FISH-FACS) methods are currently under development in our laboratory for this objective. Coupled with an automated detection and recognition procedure of the objects in ultrathin sections, an improved "microscomics" approach will help to catalog the complete gut-derived microbiome composition. Ultimately, "microscomics" will provide a method to directly detect variations between individuals, which could be linked to symptomatic or asymptomatic diseases.

Acknowledgments

This work has benefited from the French State support, managed by the 'Agence Nationale pour la Recherche', including the "Programme d'Investissement d'avenir" under the reference Méditerranée Infection 10-IAHU-03.

Conflict of Interest

The authors declare that they have no competing interests.

Authors' Contributions

Study concept and design: EK, JPB, JB. Acquisition of data: EK, JPB, FDP, CV. Analysis and interpretation of data: JPB, EK, RAA. Drafting of the manuscript: EK, JPB, JB. Critical revision of the manuscript for important intellectual content: JPB, JB, DR. All authors read and approved the final manuscript.

References

Allen, L. Geoffrey, G., and Sima, S. 2011. Advances in applied microbiology, vol. 77. Academic Press.

Angelakis, E., Bachar, D., Henrissat, B., Armougom, F., Audoly, G., Lagier, J.C., Robert, C., and Raoult, D. 2016. Glycans affect DNA extraction and induce substantial differences in gut metagenomic studies. *Sci. Rep.* **6**, 26276.

Angelakis, E., Bibi, F., Ramasamy, D., Azhar, E.I., Jiman-Fatani, A.A., Aboushoushah, S.M., Lagier, J.C., Robert, C., Caputo, A., Yasir, M., *et al.* 2014. Non-contiguous finished genome sequence and description of *Clostridium saudii* sp. nov. *Stand. Genomic Sci.* **9**, 1–12.

Arora, H.K. and Chapman, G.B. 2000. Transmission electron microscope study of bacterial morphotypes on the anterior dorsal surface of human tongues. *Anat. Rec.* **259**, 276–287.

Auchtung, T.A., Fofanova, T.Y., Stewart, C.J., Nash, A.K., Wong, M.C., Gesell, J.R., Auchtung, J.M., Ajami, N.J., and Petrosino, J.F. 2018. Investigating colonization of the healthy adult gastrointestinal tract by fungi. *mSphere* **3**, e00092-18.

Bauer, H., Sigarlakie, E., and Faure, J.C. 1975. Scanning and transmission electron microscopy of three strains of Bifidobacterium. *Can. J. Microbiol.* **21**, 1305–1316.

Breznak, J.A. and Pankratz, H.S. 1977. *In situ* morphology of the gut microbiota of wood-eating termites [*Reticulitermes flavipes* (Kollar) and *Coptotermes formosanus* Shiraki]. *Appl. Environ. Microbiol.* **33**, 406–426.

Browne, H.P., Forster, S.C., Anonye, B.O., Kumar, N., Neville, B.A., Stares, M.D., Goulding, D., and Lawley, T.D. 2016. Culturing of 'unculturable' human microbiota reveals novel taxa and extensive sporulation. *Nature* **533**, 543–546.

Clemente, J.C., Ursell, L.K., Parfrey, L.W., and Knight, R. 2012. The impact of the gut microbiota on human health: an integrative view. *Cell* **148**, 1258–1270.

Connolly, G.M., Ellis, D.S., Williams, J.E., Tovey, G., and Gazzard, B.G. 1991. Use of electron microscopy in examination of faeces and rectal and jejunal biopsy specimens. *J. Clin. Pathol.* **44**, 313–316.

Costerton, J.W. 1979. The role of electron microscopy in the elucidation of bacterial structure and function. *Annu. Rev. Microbiol.* **33**, 459–479.

Danczak, R.E., Johnston, M.D., Kenah, C., Slattery, M., Wrighton, K.C., and Wilkins, M.J. 2017. Members of the Candidate Phyla Radiation are functionally differentiated by carbon- and nitrogen-cycling capabilities. *Microbiome* **5**, 112.

Dao, M.C., Everard, A., Aron-Wisnewsky, J., Sokolovska, N., Prifti, E., Verger, E.O., Kayser, B.D., Levenez, F., Chilloux, J., Hoyles, L., *et al.* 2016. *Akkermansia muciniphila* and improved metabolic health during a dietary intervention in obesity: relationship with gut microbiome richness and ecology. *Gut* **65**, 426–436.

Earle, K.A., Billings, G., Sigal, M., Lichtman, J.S., Hansson, G.C., Elias, J.E., Amieva, M.R., Huang, K.C., and Sonnenburg, J.L. 2015. Quantitative imaging of gut microbiota spatial organization. *Cell Host Microbe* **18**, 478–488.

Ferreira-Halder, C.V., Faria, A.V.S., and Andrade, S.S. 2017. Action and function of *Faecalibacterium prausnitzii* in health and disease. *Best Pract. Res. Clin. Gastroenterol.* **31**, 643–648.

Forde, B.M., Neville, B.A., O'Donnell, M.M., Riboulet-Bisson, E., Claesson, M.J., Coghlan, A., Ross, R.P., and O'Toole, P.W. 2011. Genome sequences and comparative genomics of two *Lactobacillus ruminis* strains from the bovine and human intestinal tracts. *Microb. Cell Fact.* **10**(Suppl 1), S13.

Fuerst, J.A. and Sagulenko, E. 2011. Beyond the bacterium: planctomycetes challenge our concepts of microbial structure and function. *Nat. Rev. Microbiol.* **9**, 403–413.

Gatson, J.W., Benz, B.F., Chandrasekaran, C., Satomi, M., Venkateswaran, K., and Hart, M.E. 2006. *Bacillus tequilensis* sp. nov., isolated from a 2000-year-old Mexican shaft-tomb, is closely related to *Bacillus subtilis*. *Int. J. Syst. Evol. Microbiol.* **56**, 1475–1484.

Geva-Zatorsky, N., Alvarez, D., Hudak, J.E., Reading, N.C., Erturk-Hasdemir, D., Dasgupta, S., von Andrian, U.H., and Kasper, D.L. 2015. *In vivo* imaging and tracking of host-microbiota interactions via metabolic labeling of gut anaerobic bacteria. *Nat. Med.* **21**, 1091–1100.

Holdeman, L.V., Good, I.J., and Moore, W.E. 1976. Human fecal flora: variation in bacterial composition within individuals and a possible effect of emotional stress. *Appl. Environ. Microbiol.* **31**, 359–375.

Hovind-Hougen, K., Birch-Andersen, A., Henrik-Nielsen, R., Orholm, M., Pedersen, J.O., Teglbjaerg, P.S., and Thaysen, E.H. 1982. Intestinal spirochetosis: morphological characterization and cultivation of the spirochete *Brachyspira aalborgi* gen. nov., sp. nov. *J. Clin. Microbiol.* **16**, 1127–1136.

Hugon, P., Lagier, J.C., Colson, P., Bittar, F., and Raoult, D. 2017. Repertoire of human gut microbes. *Microb. Pathog.* **106**, 103–112.

Hugon, P., Lagier, J.C., Robert, C., Lepolard, C., Papazian, L., Musso, D., Vialettes, B., and Raoult, D. 2013. Molecular studies neglect apparently Gram-negative populations in the human gut microbiota. *J. Clin. Microbiol.* **51**, 3286–3293.

Ivanova, N., Sikorski, J., Jando, M., Munk, C., Lapidus, A., Glavina Del Rio, T., Copeland, A., Tice, H., Cheng, J.F., Lucas, S., *et al.* 2010. Complete genome sequence of *Geodermatophilus obscurus* type strain (G-20^T). *Stand. Genomic Sci.* **2**, 158–167.

Lagier, J.C., Armougom, F., Million, M., Hugon, P., Pagnier, I., Robert, C., Bittar, F., Fournous, G., Gimenez, G., Maraninchi, M., *et al.* 2012. Microbial culturomics: paradigm shift in the human gut microbiome study. *Clin. Microbiol. Infect.* **18**, 1185–1193.

Lagier, J.C., Drancourt, M., Charrel, R., Bittar, F., La Scola, B., Ranque, S., and Raoult, D. 2017. Many more microbes in humans: enlarging the microbiome repertoire. *Clin. Infect. Dis.* **65**, S20–S29.

Lagier, J.C., Hugon, P., Khelaifia, S., Fournier, P.E., La Scola, B., and Raoult, D. 2015. The rebirth of culture in microbiology through the example of culturomics to study human gut microbiota. *Clin. Microbiol. Rev.* **28**, 237–264.

Lagier, J.C., Khelaifia, S., Alou, M.T., Ndongo, S., Dione, N., Hugon, P., Caputo, A., Cadoret, F., Traore, S.I., Seck, E.H., *et al.* 2016.

Culture of previously uncultured members of the human gut microbiota by culturomics. *Nat. Microbiol.* **1**, 16203.

Leite, C.A.C., Fagundes-Neto, U., and Haapalainen, E.F. 2013. Evaluation of the ultrastructure of the small intestine of HIV infected children by transmission and scanning electronic microscopy. *Arq. Gastroenterol.* **50**, 70–77.

Lloyd-Price, J., Abu-Ali, G., and Huttenhower, C. 2016. The healthy human microbiome. *Genome Med.* **8**, 51.

Mantani, Y., Ito, E., Nishida, M., Yuasa, H., Masuda, N., Qi, W.M., Kawano, J., Yokoyama, T., Hoshi, N., and Kitagawa, H. 2015. Ultrastructural study on the morphological changes in indigenous bacteria of mucous layer and chyme throughout the rat intestine. *J. Vet. Med. Sci.* **77**, 1121–1128.

McLean, J.S., Bor, B., To, T.T., Liu, Q., Kerns, K.A., Solden, L., Wrighton, K., He, X., and Shi, W. 2018. Evidence of independent acquisition and adaption of ultra-small bacteria to human hosts across the highly diverse yet reduced genomes of the phylum Saccharibacteria. *bioRxiv*, 258137.

Meeske, A.J., Rodrigues, C.D.A., Brady, J., Lim, H.C., Bernhardt, T.G., and Rudner, D.Z. 2016. High-throughput genetic screens identify a large and diverse collection of new sporulation genes in *Bacillus subtilis*. *PLoS Biol.* **14**, e1002341.

Nash, A.K., Auchtung, T.A., Wong, M.C., Smith, D.P., Gesell, J.R., Ross, M.C., Stewart, C.J., Metcalf, G.A., Muzny, D.M., Gibbs, R.A., *et al.* 2017. The gut mycobiome of the Human Microbiome Project healthy cohort. *Microbiome* **5**, 153.

Nibali, L. and Henderson, B. 2016. The human microbiota and chronic disease: dysbiosis as a cause of human pathology. 1st edn., John Wiley & Sons Inc., Hoboken, New Jersey, USA.

O'Toole, R., Von Hofsten, J., Rosqvist, R., Olsson, P.E., and Wolf-Watz, H. 2004. Visualisation of zebrafish infection by GFP-labelled *Vibrio anguillarum*. *Microb. Pathog.* **37**, 41–46.

Paul, J., Saxena, S., and Varma, A. 1993. Ultrastructural studies of the termite (*Odontotermes obesus*) gut microflora and its cellulolytic properties. *World J. Microbiol. Biotechnol.* **9**, 108–112.

Pinos, S., Pontarotti, P., Raoult, D., Baudoin, J.P., and Pagnier, I. 2016. Compartmentalization in PVC super-phylum: evolution and impact. *Biol. Direct* **11**, 38.

Propheter, D.C. and Hooper, L.V. 2015. Bacteria come into focus: new tools for visualizing the microbiota. *Cell Host Microbe* **18**, 392–394.

Ringø, E., Lødemel, J.B., Myklebust, R., Kaino, T., Mayhew, T.M., and Olsen, R.E. 2001. Epithelium-associated bacteria in the gastrointestinal tract of Arctic charr (*Salvelinus alpinus* L.). An electron microscopical study. *J. Appl. Microbiol.* **90**, 294–300.

Ringø, E., Myklebust, R., Mayhew, T.M., and Olsen, R.E. 2007. Bacterial translocation and pathogenesis in the digestive tract of larvae and fry. *Aquaculture* **268**, 251–264.

Ringø, E., Olsen, R.E., Mayhew, T.M., and Myklebust, R. 2003. Electron microscopy of the intestinal microflora of fish. *Aquaculture* **227**, 395–415.

Santarella-Mellwig, R., Franke, J., Jaedicke, A., Gorjanacz, M., Bauer, U., Budd, A., Mattaj, I.W., and Devos, D.P. 2010. The compartmentalized bacteria of the Planctomycetes-Verrucomicrobia-Chlamydiae superphylum have membrane coat-like proteins. *PLoS Biol.* **8**, e1000281.

Sato, C., Manaka, S., Nakane, D., Nishiyama, H., Suga, M., Nishizaka, T., Miyata, M., and Maruyama, Y. 2012. Rapid imaging of mycoplasma in solution using Atmospheric Scanning Electron Microscopy (ASEM). *Biochem. Biophys. Res. Commun.* **417**, 1213–1218.

Scott, T.G., Curran, B., and Smyth, C.J. 1989. Electron microscopy of adhesive interactions between *Gardnerella vaginalis* and vaginal epithelial cells, McCoy cells and human red blood cells. *J. Gen. Microbiol.* **135**, 475–480.

Serra, C.R., Earl, A.M., Barbosa, T.M., Kolter, R., and Henriques, A.O. 2014. Sporulation during growth in a gut isolate of *Bacillus subtilis*. *J. Bacteriol.* **196**, 4184–4196.

Southern, P.M.Jr. 1975. Bacteremia due to *Succinivibrio dextrinosolvens*. Report of a case. *Am. J. Clin. Pathol.* **64**, 540–543.

Takenaka, R., Aoi, Y., Ozaki, N., Ohashi, A., and Kindaichi, T. 2018. Specificities and efficiencies of primers targeting *Candidatus* phylum Saccharibacteria in activated sludge. *Materials (Basel)* **11**, 1129.

Taras, D., Simmering, R., Collins, M.D., Lawson, P.A., and Blaut, M. 2002. Reclassification of *Eubacterium formicigenerans* Holdeman and Moore 1974 as *Dorea formicigenerans* gen. nov., comb. nov., and description of *Dorea longicatena* sp. nov., isolated from human faeces. *Int. J. Syst. Evol. Microbiol.* **52**, 423–428.

Villegas, H., Arias, F., Flores, E., Casanova, G., and Karchmer, S. 1997. Ultrastructural characteristics of *Gardnerella vaginalis* infection in the heterosexual couple. *Arch. Androl.* **39**, 147–153.

Walker, C.A., Gómez, B.L., Mora-Montes, H.M., Mackenzie, K.S., Munro, C.A., Brown, A.J.P., Gow, N.A.R., Kibbler, C.C., and Odds, F.C. 2010. Melanin externalization in *Candida albicans* depends on cell wall chitin structures. *Eukaryot. Cell* **9**, 1329–1342.

Weir, T.L., Manter, D.K., Sheflin, A.M., Barnett, B.A., Heuberger, A.L., and Ryan, E.P. 2013. Stool microbiome and metabolome differences between colorectal cancer patients and healthy adults. *PLoS One* **8**, e70803.

Whitman, W.B., Coleman, D.C., and Wiebe, W.J. 1998. Prokaryotes: The unseen majority. *Proc. Natl. Acad. Sci. USA* **95**, 6578–6583.